Bioconjugate Chemistry

Article

pubs.acs.org/bc

Multifunctional DNA-Gold Nanoparticles for Targeted Doxorubicin Delivery

Colleen M. Alexander, Kristen L. Hamner, Mathew M. Maye,* and James C. Dabrowiak*

Department of Chemistry, Syracuse University, 111 College Place, Syracuse, New York 13244-4100, United States

Supporting Information

ABSTRACT: In this report we describe the synthesis, characterization, and cytotoxic properties of DNA-capped gold nanoparticles having attached folic acid (FA), a thermoresponsive polymer (*p*), and/or poly(ethylene glycol) (PEG) oligomers that could be used to deliver the anticancer drug doxorubicin (DOX) in chemotherapy. The FA-DNA oligomer used in the construction of the delivery vehicle was synthesized through the reaction of the isolated folic acid *N*-hydroxysuccinimide ester with the amino-DNA and the conjugated DNA product was purified using high performance liquid chromatography (HPLC). This approach ultimately allowed control of the amount of FA attached to the surface of the delivery vehicle. Cytotoxicity studies using SK-N-SH neuroblastoma cells with drug loaded delivery vehicles were carried out using a variety of exposure times (1−48 h) and recovery times (1−72 h), and in order to access the effects of varying amounts of attached FA, in culture media deficient in FA. DOX loaded delivery vehicles having 50% of the DNA strands with attached FA were more cytotoxic than when all of the strands contained FA. Since FA stimulates cell growth, the reduced cytotoxicity of vehicles fully covered with FA suggests that the stimulatory effects of FA can more than compensate for the cytotoxic effects of the drug on the cell population. While attachment of hexa-ethylene glycol PEG(18) to the surface of the delivery vehicle had no effect on cytotoxicity, 100% FA plus the thermoresponsive polymer resulted in IC_{50} = 0.48 ± 0.01 for an exposure time of 24 h and a recovery time of 1 h, which is an order of magnitude more cytotoxic than free DOX. Confocal microscopic studies using fluorescence detection showed that SK-N-SH neuroblastoma cells exposed to DOX-loaded vehicles have drug accumulation inside the cell and, in the case of vehicles with attached FA and thermoresponsive polymer, the drug appears more concentrated. Since the biological target of DOX is DNA, the latter observation is consistent with the high cytotoxicity of vehicles having both FA and the thermoresponsive polymer. The study highlights the potential of DNA-capped gold nanoparticles as delivery vehicles for doxorubicin in cancer chemotherapy.

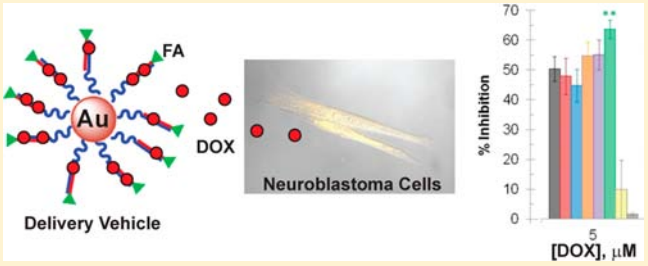

INTRODUCTION

Gold nanoparticles (AuNP) are being widely developed as new treatment and diagnostic agents in medicine. The intense interest in the medical applications of AuNP stems from their inherently low cytotoxicities, easily controlled sizes and shapes, and surface properties that allow attachment of a wide variety of organic groups and ligands.[1−7] Gold nanoparticles are particularly useful for detecting and treating cancer largely because they can passively target tumor tissue via the enhanced permeability and retention (EPR) effect. Since tumor vasculature contains voids between the endothelial cells that are larger than those found in healthy tissue, particles in the size range ∼6−200 nm can pass through the voids and become momentarily trapped in the extracellular matrix.[3,8] This provides an advantage for a suitably equipped nanoparticle to release its cytotoxic drug cargo within the tumor mass.

An important goal of cancer chemotherapy is to enhance the selectivity of the drug or cytotoxic agent toward cancer cells while minimizing the damage that it may cause to healthy cells.[9,10] Since many copies of the same or different ligands can be attached to the surface of AuNP, a single nanoparticle can be equipped not only with cytotoxic and sensing agents but also with groups capable of targeting certain cell types.[11−14] An example of this type of targeting vector is the integrin-binding arginylglycylaspartic acid (RGD) tripeptide that has been incorporated into a range of nanoparticle vehicles.[15−17] Gold nanoparticles having attached sensitizing dyes have potential in photodynamic therapy (PDT).[18−20] In addition to the tripeptide RGD, gold nanoparticles having the surface-attached targeting peptide epidermal growth factor (EGF) and the sensitizing dye phthalocyanine 4 are useful for treating cancerous brain cells in PDT.[21]

Folic acid (FA), or vitamin B_9, is necessary for mammalian cell growth.[22] Since FA has a high binding affinity for the folic acid receptor, FR ($K_d \approx 1 \times 10^{-10}$ M), which is overexpressed on the surface of certain cancer cells, the vitamin is a useful vector for incorporation into nanoparticle drug delivery vehicles.[23−27] Nanoparticles with attached FA enter the cell

Received: March 27, 2014
Revised: May 31, 2014
Published: June 9, 2014

Scheme 1. Synthesis and Isolation of the DNA–Folic Acid Conjugate, 1b-FA, and Its Incorporation into the Delivery Vehicle to Yield 1ab-FA-AuNP[a]

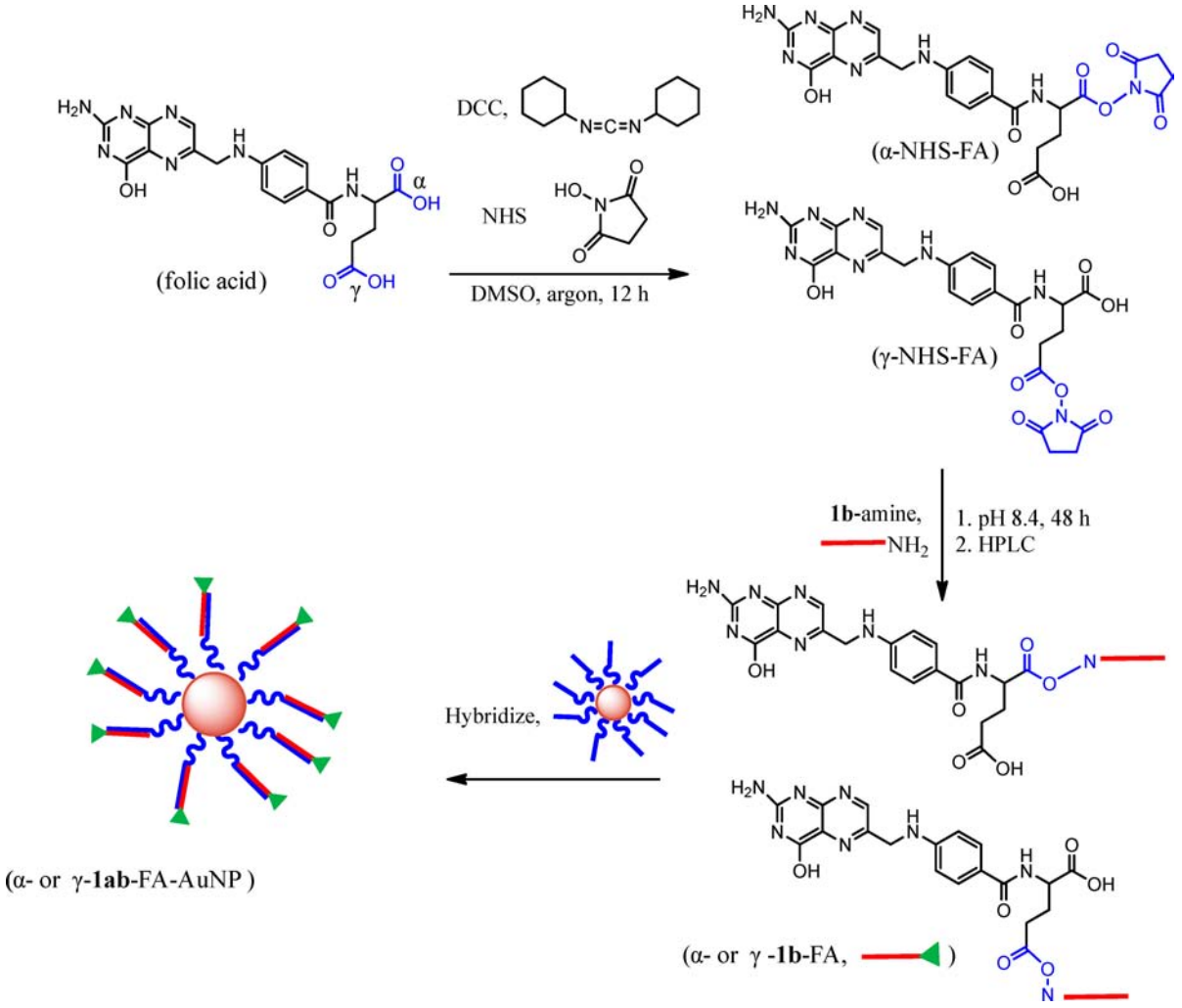

[a]The blue line represents the thiolated 35-mer, **1a**, 5′-HS$(CH_2)_6T_{15}$ TGT TCG TAT TCG TAT TCG TC, and the red line represents its partial complement, the 19-mer, **1b**, 5′-GAG GAA TAC GAA TAC GAA C. DOX binding sites are underlined.

via receptor mediated endocytosis bringing with them their toxic drug payload for killing the cell.

A front line anticancer drug often incorporated into nanoparticle drug delivery vehicles is doxorubicin (DOX).[28,29] We previously described the synthesis and characterization of gold nanoparticles with attached duplex DNA capable of delivering DOX and the clinically used anticancer drug actinomycin D (ActD) to cancer cells.[30,31] Since drug loading on the nanoparticle is controlled by the number and sequence of surface attached DNA molecules and targeting vectors, and mononuclear phagocyte system (MPS) evading agents can be incorporated into the particle, the resulting assembly is a versatile vehicle for delivering clinically used DNA interacting drugs in cancer chemotherapy. In examining release mechanisms for the bound drug, we studied the ability of the particle-bound thermoresponsive polymer to affect the binding constant and release kinetics of DOX from the nanoparticle.[32] We found that changing temperature causes the polymer shell to undergo a hydrophilic–phobic phase transition that influences the binding constant and the rate of release of the anticancer drug from the DNA-AuNP.

In this report we describe the synthesis and characterization of AuNP delivery vehicles having surface bound duplex DNA equipped with folic acid (Scheme 1), a thermoresponsive polymer, and PEG oligomers. To control the number of FA molecules bound to the nanoparticle surface and determine cytotoxicity as a function of FA surface concentration, we synthesized and purified a folic acid DNA oligomer that was incorporated into the final assembly. The cytotoxicity of the DOX loaded delivery vehicles toward neuroblastoma (SK-N-SH) cells and the results of confocal imaging studies are also reported and discussed in this work.

RESULTS AND DISCUSSION

A two step approach was employed in order to covalently attach FA to the complementary oligonucleotide **1b**, yielding **1b**-FA (Scheme 1). First, FA was activated with NHS and the resulting FA-NHS was isolated and characterized. Second, the FA-NHS reaction product was reacted with **1b**-amine and HPLC-purified to yield **1b**-FA. ^1H and ^{13}C NMR showed that the FA-NHS reaction product consisted of FA derivatives containing the NHS ester group (~66%) and unreacted FA (~34%) (Figure 1 and Table S1, Supporting Information).

dx.doi.org/10.1021/bc500136r | Bioconjugate Chem. 2014, 25, 1261–1271

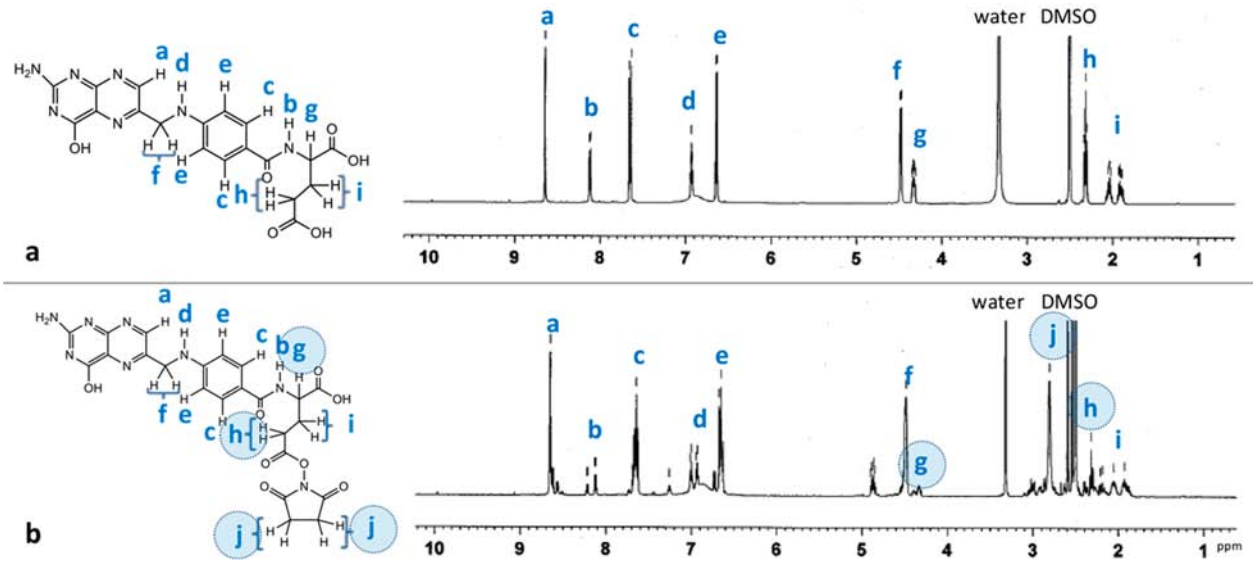

Figure 1. 300 MHz ^{1}H NMR spectra of (a) FA and (b) NHS-FA (γ isomer shown) in DMSO-d_6.

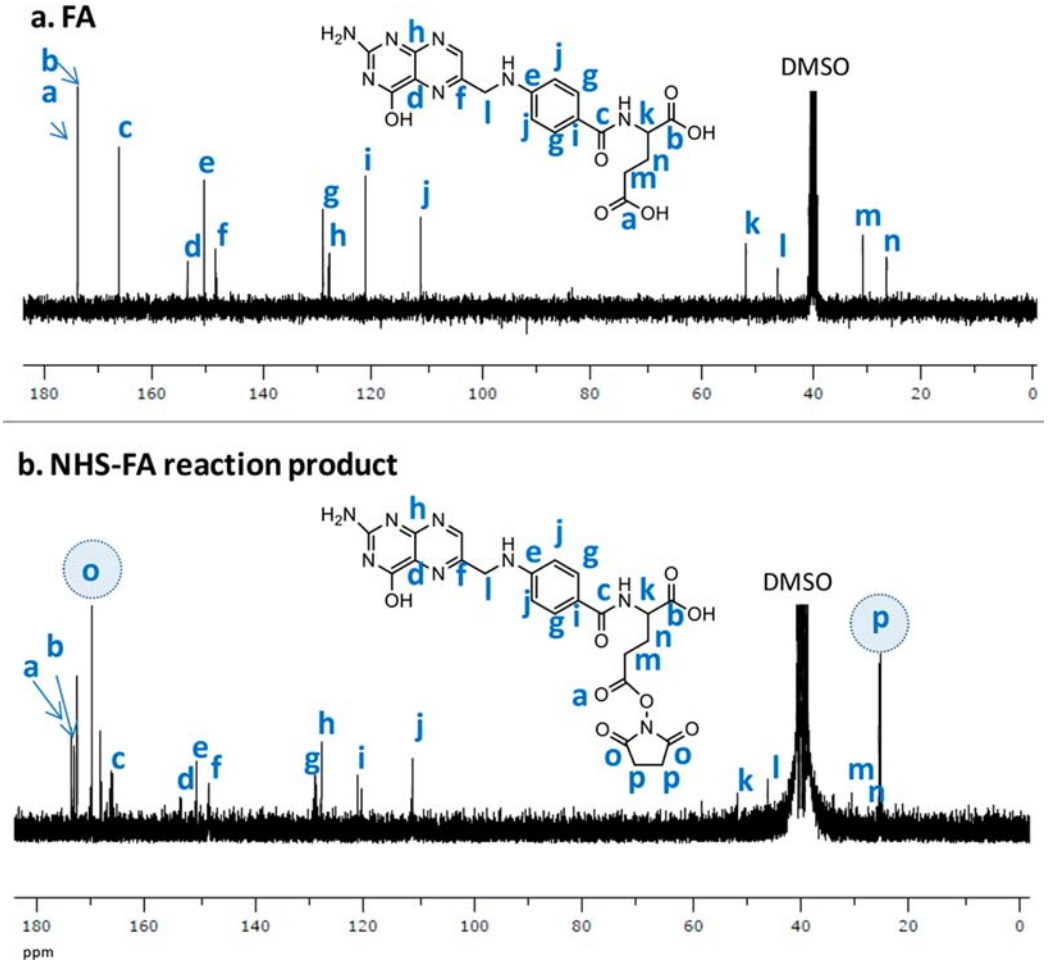

Figure 2. ^{13}C NMR spectra of (a) FA and (b) NHS-FA (γ isomer shown) in DMSO-d_6.

Integration of the proton resonances in Figure 1 showed that peaks **h** (the methylene protons of FA) and **g** (methine proton in the glutamate portion of FA) of folic acid decrease by ∼66% each, which is consistent with NHS ester formation at the γ and α carboxylates of FA. Furthermore, a new peak **j** (the methylene protons of the NHS residue) appeared in the spectrum of the NHS-FA reaction product having an integration of 2.6 H. Since this resonance should integrate for 4 H, if all of the FA in the reaction was converted to NHS esters, the mixture contains ∼65% NHS-FA.

Figure 2 shows the ^{13}C NMR spectrum of FA and the NHS-FA reaction product in DMSO-d_6, with the peak assignments in

dx.doi.org/10.1021/bc500136r | *Bioconjugate Chem.* 2014, 25, 1261−1271

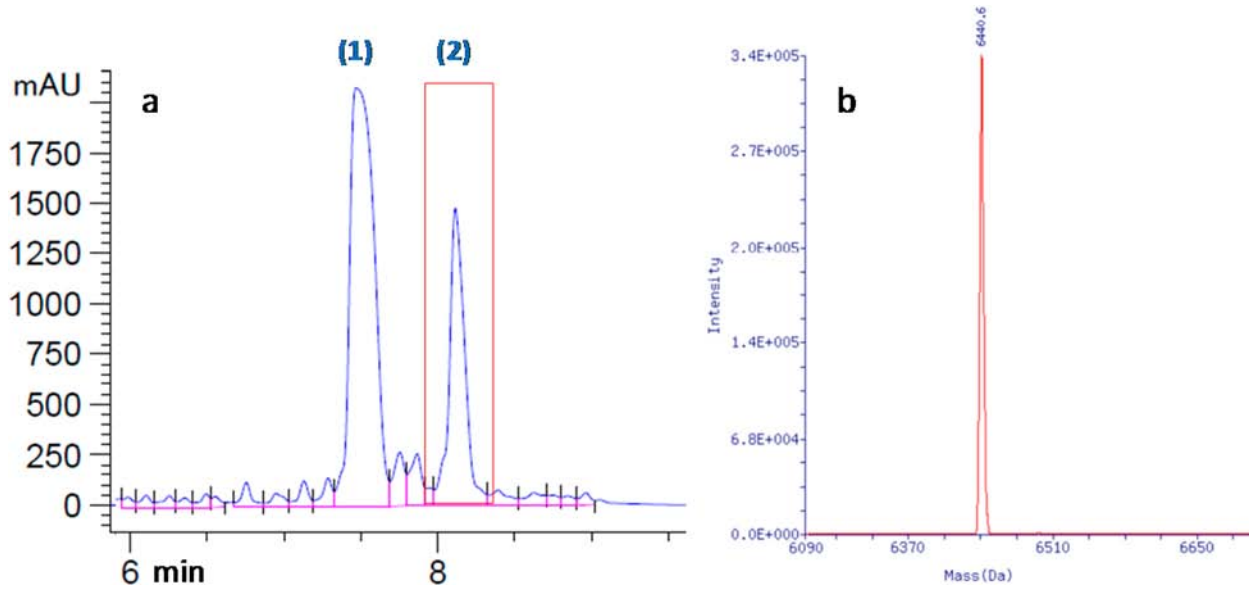

Figure 3. (a) IE-HPLC chromatogram of the reaction mixture showing (1) **1b**-amine and (2) **1b**-FA. The red rectangle indicates the fraction collection window for **1b**-FA. (b) Molecular ion **1b**-FA molecular weight (6440.6) by ESI-MS.

Table S2 of the Supporting Information. The presence NHS esters in the reaction product is indicated by peaks **o** and **p** in Figure 2b, which correspond to carbonyl (amide) and methylene carbons of NHS, respectively. Also, since peaks **a**, **b**, **m**, **n**, and **k** have reduced intensity relative to those of FA (Figure 2a), these resonances have been shifted to new positions in the spectrum of the reaction product, Figure 2b. Additional characterization of the NHS-FA reaction product includes FT-IR (Figure S1 and Table S3) and ESI-MS (Figure S2), in the Supporting Information

The NHS-FA reaction product (containing ~66% NHS-FA) was reacted with **1b**-amine to produce a mixture of compounds containing unreacted **1b**-amine and **1b**-FA. Since **1b**-amine and **1b**-FA have different total net charges, −18 and −20, respectively, ion exchange high performance liquid chromatography (IE-HPLC) was used to separate the mixture on the basis of molecular charge. As shown in Figure 3a, the faster eluting peak identified as **1b**-amine, peak (1) (retention time 7.48 min) exhibits baseline separation from the slower eluting compound **1b**-FA, peak (2) (retention time 8.12 min). Following multiple injections and collection of fractions in the time domain indicated by the rectangle in Figure 3a, **1b**-FA was recovered from the pooled fractions by ethanol precipitation and its mass determined using ESI-MS, m/z observed, 6440.6, calculated, 6441.

Considering that fraction collection was limited to only the **1b**-FA peak, and the peak has a symmetrical appearance, without shoulders (Figure 3a), it seems unlikely that other molecules coeluted with **1b**-FA. However, considering that an approximately 1:1 mixture of both α-NHS-FA and γ-NHS-FA were reacted with **1b**-amine, we assume that the HPLC separated material contains both α- and γ-**1b**-FA.

The folic acid conjugate, **1b**-FA, was also characterized by UV−vis spectrophotometry. As expected, the spectrum of **1b**-FA is essentially a sum of the spectra of **1b**-amine and FA (Figure 4). Specifically, the **1b**-FA spectrum contains a narrow peak at $\lambda_{max} \approx 260$ nm, characteristic of DNA, and a broad weak peak at ~350 nm, characteristic of FA. The DNA peak in the **1b**-FA spectrum (i) is slightly red-shifted at 259.5 nm in

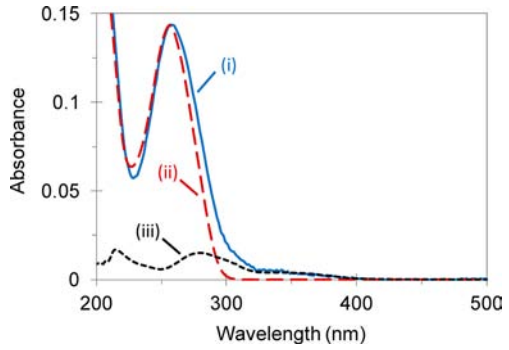

Figure 4. UV−vis spectra for purified **1b**-FA (i) compared to **1b**-amine (ii) and free FA (iii).

comparison to the DNA peak of **1b**-amine (ii) at 256.5 nm. The broad FA peak at ~350 nm in the **1b**-FA spectrum is consistent in appearance with the same peak in the free FA spectrum (iii) showing that the DNA and FA chromophores are essentially additive.

Throughout these studies, several batches of **1ab**-FA-AuNP were prepared by hybridizing **1a**-AuNP with varying purities of **1b**-FA. The three most noteworthy batches, discussed here, involve hybridization of **1a**-AuNP with **1b**-(8%)FA, **1b**-(50%)FA, and **1b**-(100%)FA, where the listed percentage indicates the percent of **1b** bound to FA. For example, **1b**-(50%)FA consists of 50% **1b**-FA and 50% **1b**-amine. Hybridization therefore resulted in the synthesis of **1ab**-(8%)FA-AuNP, **1ab**-(50%)FA-AuNP, and **1ab**-(100%)FA-AuNP. Using a CY3-modified **1b**, the number of DNA duplexes bound per AuNP was determined to be 63.7 ± 2.0 for the **1ab**-(8%)FA-AuNP batch and 65.4 ± 1.3 for the other two batches. Considering the number of bound duplexes and the percent of DNA bound to FA, the total number of FA molecules bound per **1ab**-(8%)FA-AuNP, **1ab**-(50%)FA-AuNP, and **1ab**-(100%)FA-AuNP are therefore ~5, ~33, and ~65, respectively. Figure S3 (Supporting Information) shows the UV−vis spectra for the three folic acid modified DNA-AuNP batches. An additional form of characterization

dx.doi.org/10.1021/bc500136r | *Bioconjugate Chem.* 2014, 25, 1261−1271

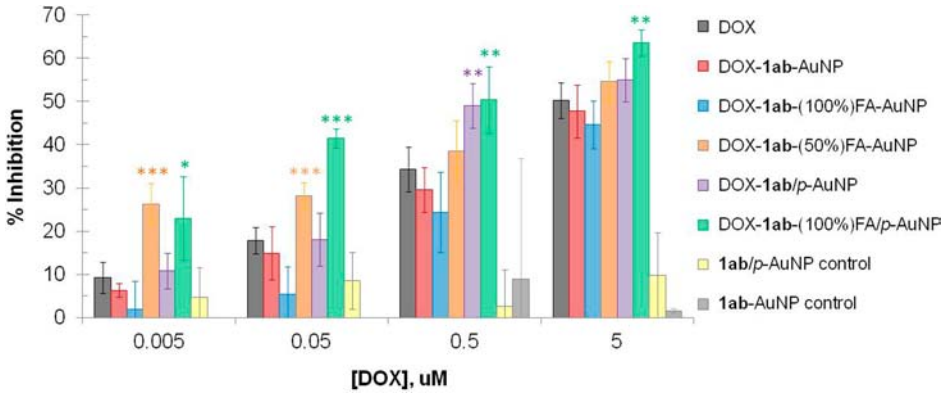

Figure 5. Percent inhibition of neuroblastoma cells exposed to varying drug conditions for 24 h. For **1ab**-AuNP in the absence of DOX, cells were exposed to vehicle for 48 h at 0.05, 0.5, and 5 μM effective DOX.[31] Asterisks: experimental %*I* significantly exceeds corresponding DOX %*I*, at $p < 0.05$ (*), $p < 0.005$ (**), or $p < 0.0005$ (***) for a one-tailed *t* test.

performed for the **1ab**-(100%)FA-AuNP was dynamic light scattering (DLS). The hydrodynamic diameter, D_h, was measured to be 26.4 ± 0.4 nm for **1ab**-(100%)FA-AuNP, compared to 23.0 ± 1.5 nm for a **1ab**-AuNP control. Both samples were prepared using the same **1a**-AuNP batch and the same experimental conditions, other than hybridization with **1b**-(100%)FA instead of **1b** for **1ab**-(100%)FA-AuNP. Therefore, the increase in particle D_h, ΔD_h, due to the attachment of FA is 3.4 ± 1.6 nm (error obtained by propagation). This diameter may be divided by two, to convert to a radius, 1.7 ± 0.8 nm, which is very reasonable as the hydrodynamic length of FA.

In order to control the kinetic and equilibrium properties of DOX release, the **1ab**-AuNP was functionalized with a thermoresponsive pNIPAAm-*co*-pAAm polymer, *p*. The polymer, *p*, undergoes a transition at its critical temperature, T_c of 53 °C, wherein the polymer is hydrophilic and extended at $T <$ 53 °C, and hydrophobic and condensed at $T >$ 53 °C.[32] We recently reported the characterization of **1ab**/*p*-AuNP by dialysis, which quantified the kinetics (as off-rate constant, β) and equilibrium (as equilibrium constant, *K*) of drug release.[32] These results supported the hypothesis that at physiological temperature (37 °C, $<T_c$), the extended form of *p* sterically inhibits DOX release and elevates the binding constant, *K*. Here, we also report the hydrodynamic diameters of these particles at $T > T_c$ and $T < T_c$, as measured by DLS (Table S4, Supporting Information). There is a ∼30 nm increase in the D_h of **1ab**/*p*-AuNP at $T < T_c$ (relative to $T > T_c$), which corresponds to ∼15 nm of additional hydrodynamic shell through which the drug must diffuse for complete dissociation from the nanoparticle.

Functionalizing AuNP with poly(ethylene glycol) (PEG) has been shown to prevent the mononuclear phagocyte system (MPS) from recognizing the particle which increases the circulation time of the AuNP in the bloodstream.[33] In order to examine the effect of PEG on the cytotoxicity of the delivery vehicle, the 5′ end of the solvent directed strand of **1ab**-AuNP was modified with either the triethylene glycol, PEG(9), or hexa-ethylene glycol, PEG(18). These delivery vehicles were synthesized by hybridizing PEG(9)- or PEG(18)-**1b** with **1a**-AuNP to produce **1ab**-PEG(9)- or **1ab**-PEG(18)-AuNP. As expected, the UV−vis spectra of **1ab**-(PEG9)-AuNP and **1ab**-(PEG18)-AuNP are identical (Figure S4, Supporting Information). The hydrodynamic diameters, D_h, for **1ab**-(PEG9)-AuNP and **1ab**-(PEG18)-AuNP are 23.7 ± 1.8 nm and 24.7 ± 1.4 nm, respectively.

Since doxorubicin is clinically used for treating neuroblastoma, a cancer of the involuntary nervous system,[34−36] neuroblastoma (SK-N-SH) cells were utilized to evaluate the cytotoxicity of the various vehicles. In assessing the ability of FA to serve as a targeting vector, cells were initially grown in media containing FA, but one cell passage prior to the intended cytotoxicity experiments, the cells were grown in media containing no folic acid. This approach[37−39] allows the cells to initially grow in the normal manner in a folic acid-rich environment and then, through the FA deficient step, sensitizes them to the uptake of FA. Since the time required for the folic acid receptor (FR) to bind its cargo on the cell surface, internalize into the cell, and return to the surface is 8−12 h,[26] one passage of the SK-N-SH cells (∼4 days) was regarded as a sufficient time to clear all FA from the system and not significantly affect the general health of the population.

Figure 5 summarizes the cytotoxicity results, as percent inhibition (%*I*) of neuroblastoma cells as a function of DOX concentration for seven conditions. The IC_{50} values were estimated by extrapolation of the trends in Figure 5.[31] It can be observed that the IC_{50} values of DOX (black, 4.94 ± 0.01 μM) and DOX-**1ab**-AuNP (red, 5.56 ± 0.04 μM) produce the same trend as previously reported,[31] i.e., free DOX is more cytotoxic than DOX-**1ab**-AuNP. In these IC_{50} values the error bars represent the errors in fit to the inhibition plots, and not multiple experiments.

Interestingly, DOX-**1ab**-(100%)FA-AuNP (blue), the vehicle for which all duplex DNA strands have solvent directed FA, showed generally lower inhibition (less cytotoxicity) than DOX-**1ab**-AuNP. Since equipping the particle with FA would lead to greater DOX uptake, this result is surprising. If the amount of FA on the particle is reduced, as in the case with DOX-**1ab**-(50%)FA-AuNP (tan), cytotoxicity significantly increases (IC_{50} = 3.72 ± 0.01 μM) compared to DOX-**1ab**-(100%)FA-AuNP (IC_{50} = 9.3 ± 0.1 μM) (Figure 6). The dependency of cytotoxicity on FA coverage may be due to the interplay of the growth-enhancing effect of FA and the lethality of DOX. When FA-deprived cells are exposed to DOX-loaded particles having a high concentration of surface attached FA (e.g., for DOX-**1ab**-(100%)FA-AuNP), the cell growth stimulation effects of folic acid could outweigh the cytotoxic effects of the drug. Further study will be needed to determine if

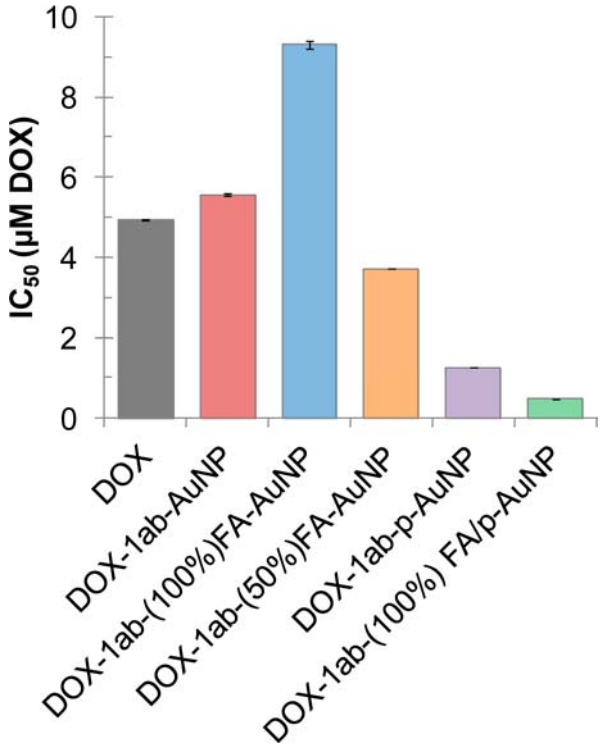

Figure 6. Summary of IC_{50} values for neuroblastoma SK-N-SH cells exposed to varying drug conditions for 24 h, with 1 h recovery.

in fact FA conjugated to the DNA-AuNP can serve as a nutrient to the cells, similarly to free FA.

The effects of incorporating *p* into the vehicle are shown in Figure 5. DOX-**1ab**/*p*-AuNP shows similar cytotoxicity to free DOX at the two lowest concentrations, but shows greater inhibition than DOX at the two highest concentrations. This condition produced an extremely low IC_{50} value of 1.25 ± 0.01 μM, which is lower than free DOX, DOX-**1ab**-AuNP, and even the two FA-modified vehicles. Since recently published studies[32] show that the surface attached polymer increases the binding constant of DOX for its binding sites on surface attached duplex DNA, the enhanced cytotoxicity observed for DOX-**1ab**/*p*-AuNP could be due to more DOX remaining on the particle through the cell internalization process.

In another important cytotoxicity condition, FA and *p* were both incorporated into the vehicle. Figure 5 shows that DOX-**1ab**-(100%)FA/*p*-AuNP exhibits statistically elevated inhibition compared to DOX at all concentrations. This particular vehicle seems to display the advantages of both FA modification (elevated inhibition at low concentrations) and *p* modification (elevated inhibition at high concentrations), resulting in an IC_{50} = 0.482 ± 0.001 μM, which is significantly lower than all other conditions explored thus far (Figure 6).

Finally, Figure 5 also shows that inhibition of neuroblastoma cells by a **1ab**/*p*-AuNP control in the absence of DOX is relatively minimal. The %*I* only slightly exceeds zero when considering error. This demonstrates that incorporation of *p* into the vehicle does not introduce prohibitively high cytotoxicity.

Cytotoxicity results across several experiments are summarized in Table 1. Nine different drug conditions and four different exposure/recovery conditions are represented. The table summarizes the IC_{50} values for each condition. Furthermore, the table summarizes for each experimental condition the factor of IC_{50} decrease compared to its corresponding DOX condition. This was calculated in order to enable fair comparisons across experiments.

Table 1 shows that the IC_{50} values for DOX range from a minimum of ∼0.04 μM at an exposure and recovery time (E/R) of 48/1 (48 h/1 h) to a maximum of ∼5.6 μM at E/R = 1/72, 5/72, 24/1. This data also reflects the general trend that measured IC_{50} values are inversely related to exposure time. This is anticipated, as increasing the exposure time would result in more drug−cell interactions and logically less drug required to kill cells. In comparison to DOX, the IC_{50} values for DOX-**1ab**-AuNP are consistently slightly higher (Table 1). At E/R times of 1/72, 5/72, 24/1, and 48/1, the factor decrease in IC_{50} for DOX-**1ab**-AuNP is consistently less than one, with values ranging 0.2−0.8. In general, DOX-**1ab**-AuNP may therefore be regarded as less cytotoxic toward neuroblastoma cells than free DOX.

The delivery vehicle DOX-**1ab**(PEG18)-AuNP, with PEG18 incorporated into the assembly, has the same IC_{50} value as that of DOX-**1ab**-AuNP (Table 1). This indicates that PEG could be incorporated into the vehicle for MPS evasion without significantly affecting the drug delivery performance of the vehicle. However, animal studies would be required to evaluate the effectiveness of a PEG-modified vehicle in evading the MPS system and lengthening blood circulation times.

Table 1. Summary of IC_{50} Values (μM) across Several Cytotoxicity Experiments at Varying Exposure and Recovery (E/R) Times[a]

					DOX-1ab-FA			DOX-1ab-FA/p-AuNP	
E/R (h)	DOX	DOX-1ab-AuNP	DOX-1ab-PEG18-AuNP	DOX-1ab/*p*-AuNP	100% FA	50% FA	8% FA	100% FA	8% FA
1/72	≫2.5	5.13 ± 1.52							
5/72	1.28 ± 0.02	5.57 ± 0.09 (0.2)							
24/1	4.94 ± 0.01	5.56 ± 0.04 (0.9)		1.25 ± 0.01 (4.0)	9.3 ± 0.1 (0.5)	3.72 ± 0.01 (1.3)		0.48 ± 0.01 (10.3)	
24/1	2.81 ± 1.55	5.58 ± 1.12 (0.5)							
24/1	2.15 ± 0.01	4.37 ± 0.03 (0.5)		0.43 ± 0.16 (5.0)			1.93 ± 0.01 (1.1)		0.33 ± 0.01 (6.5)
48/1	0.04 ± 0.02	0.05 ± 0.02 (0.8)	0.05 ± 0.02 (0.8)						

[a]The factor by which IC_{50} decreases relative to the corresponding DOX condition is indicated in parentheses.

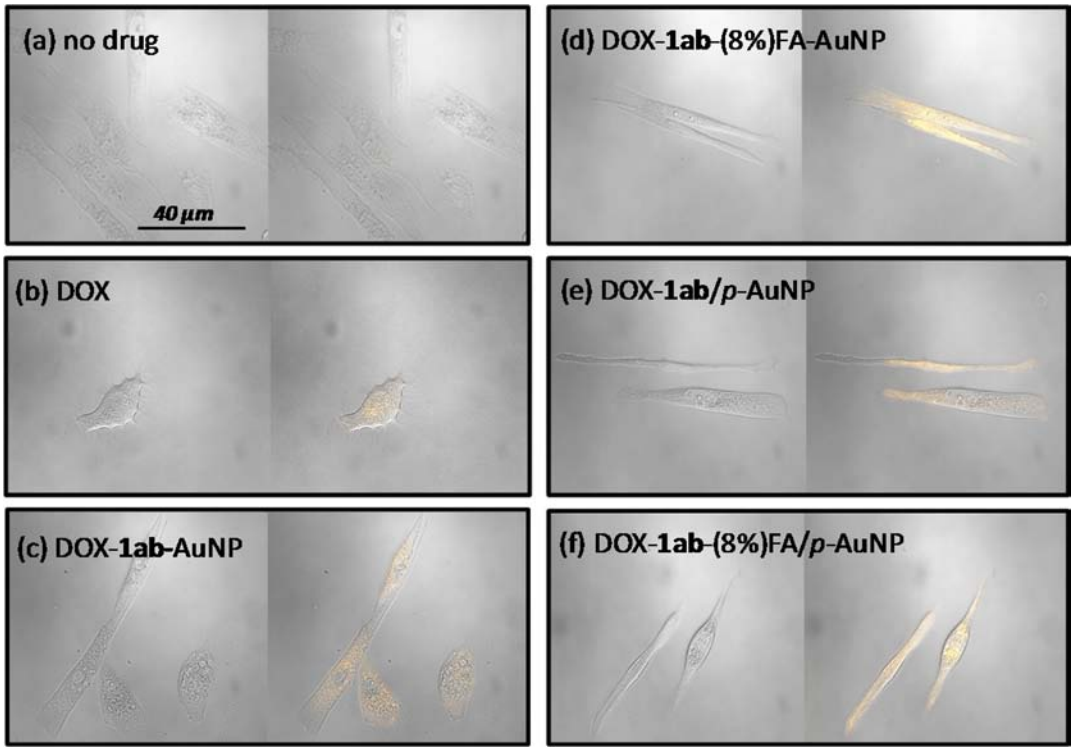

Figure 7. Confocal images of neuroblastoma cells exposed to (a) no drug, (b) 5 μM of DOX, (c) DOX-**1ab**-AuNP, (d) DOX-**1ab**-8%FA-AuNP, (e) DOX-**1ab**/*p*-AuNP, and (f) DOX-**1ab**-8%FA/*p*-AuNP. The images consist of a brightfield (left) and DOX fluorescence+brightfield (right); scale bar in (a) applies to all of the images shown.

The thermoresponsive vehicle DOX-**1ab**/*p*-AuNP was employed in two cytotoxicity experiments at E/R = 24/1, both of which displayed significantly enhanced cytotoxicity relative to DOX by a factor of 4 or 5. The enhanced cytotoxicity of DOX-**1ab**/*p*-AuNP seems to result from the improved binding constant, *K*, of DOX toward the vehicle. The temperature of the cell experiments, 37 °C, never exceeded T_c, the temperature at which the polymer undergoes a phase change to depress *K*. Since functionalization with *p* results in *K* elevation and IC_{50} decline, it may be the case that increasing polymer length, drug loading density, or decreasing T_c will further optimize the vehicle's drug release kinetics, equilibrium, and cytotoxic properties.

Folic acid was incorporated into the vehicle in three different loading conditions, including DOX-**1ab**-(8%)FA-AuNP, DOX-**1ab**-(50%)FA-AuNP, and DOX-**1ab**-(100%)FA-AuNP, all of which were performed at E/R = 24/1. The IC_{50} decreased for these three conditions by factors of 1.1, 1.3, and 0.5, respectively. The cytotoxicity data therefore suggests that lower FA loading densities are sufficient for targeting and enhance cytotoxicity. However, high densities of FA (100%) produce a decline in cytotoxicity. Further studies could determine the optimal FA loading for maximized targeting and minimized cell nourishment, but the optimal condition explored in this study is a moderate loading, at DOX-**1ab**-(50%)FA-AuNP.

Two conditions were explored in which the vehicle was modified with both FA and polymer. Both of these studies were performed at E/R = 24/1, with varying FA loading. For DOX-**1ab**-(8%)FA/*p*-AuNP, IC_{50} decreased compared to free DOX by a factor of 6.5, which exceeds that of the corresponding *p*- or FA-modified conditions. For the DOX-**1ab**-(100%)FA/*p*-AuNP, IC_{50} decreased by a factor of 10.3. This vehicle was the most cytotoxic explored thus far, greatly surpassing the vehicles functionalized with only *p* or FA.

Confocal microscopy was also used to study the fate of DOX after exposing the drug-loaded vehicle to neuroblastoma cells. These experiments were done using the same conditions as the corresponding cytotoxicity experiments, except that cells were seeded on Mat-tek glass-bottom culture dishes suitable for optical measurements. As with cytotoxicity experiments, cells were exposed to RPMI+ (RPMI media deficient in folic acid, containing 10% fetal bovine serum (FBS), 100 μg/mL streptomycin, and 100 IU/mL penicillin) one pass before seeding on the glass-bottom culture dish. Confocal measurements were performed using 5 μM free DOX or various delivery vehicles having 5 μM of loaded DOX, using 24 h exposure and 1 h recovery time.

Figure 7 shows confocal microscopy images from two channels (bright field, and bright field + fluorescence). In the absence of added free or particle-bound DOX (Figure 7a), the cells are elongated and stretchy, which is consistent with a healthy morphology. This condition serves as a control, and no DOX fluorescence (using (λ_{ex} = 490 nm, λ_{em} = 565−615 nm) is detected. Treatment of cells with free DOX reveals moderate DOX fluorescence (Figure 5b). When the cells are exposed to the DOX loaded vehicle having no folic acid, DOX-**1ab**-AuNP (Figure 7c), fluorescence indicates moderate drug uptake with most of the DOX localized in the cell cytoplasm rather than the nucleus. Since DOX exerts its cytotoxic effects by binding to DNA in the nucleus and subsequently inhibiting DNA replication and RNA transcription,[40] the observation that less drug distributes to the nucleus suggests that DOX-**1ab**-AuNP may be less effective than free DOX in inhibiting cell growth. Indeed, this observation is consistent with the previously

dx.doi.org/10.1021/bc500136r | *Bioconjugate Chem.* 2014, 25, 1261−1271

observed cytotoxicity trend of IC_{50}(DOX) < IC_{50}(DOX-**1ab**-AuNP).[31]

Figure 7d–f shows the confocal images for DOX-**1ab**-8%FA-AuNP, DOX-**1ab**/*p*-AuNP, and DOX-**1ab**-8%FA/*p*-AuNP. Interestingly, all three of these vehicles produce greatly enhanced DOX fluorescence throughout the cell including the nucleus. The overall trend of DOX internalization based on a qualitative estimate of drug fluorescence is DOX-**1ab**-8%FA/*p*-AuNP ≅ DOX-**1ab**-8%FA-AuNP > DOX-**1ab**/*p*-AuNP ≫ DOX > DOX-**1ab**-AuNP, with only the latter vehicle showing poor delivery of DOX to the nucleus. This suggests that modification of DOX-**1ab**-AuNP with FA and/or *p* facilitates delivery of the drug to the nucleus of the cell. Since it is known that the fluorescence of DOX is quenched when the drug is in close proximity to the gold nanoparticle,[41] observation of drug fluorescence indicates that DOX is free within the cell and no longer bound to the nanoparticle. Therefore, in the case of all DOX-loaded vehicles, the observed fluorescence intensity should be regarded as a low estimate of internalized DOX because some DOX could be inside the cell but, due to proximity-quenching by the nanoparticle, it is not observed in the drug fluorescence channel.

CONCLUSIONS

In this report we describe the synthesis and characterization of DNA-capped gold nanoparticles having attached folic acid (FA), thermoresponsive polymer (*p*), and/or poly(ethylene glycol) (PEG) oligomers that are suitable for delivering the anticancer drug doxorubicin (DOX) in chemotherapy. The FA-DNA oligomer required for constructing the vehicle was synthesized by reacting the isolated folic acid *N*-hydroxysuccinimide ester with the amino-DNA followed by HPLC purification. Confocal microscopic studies using fluorescence detection showed that SK-N-SH neuroblastoma cells exposed to DOX-loaded vehicles have drug accumulation inside the cell and, in the case of vehicles with attached FA and thermosensitive polymer, drug appears more concentrated. Cytotoxicity studies using neuroblastoma cells showed that cytotoxicity of drug-loaded vehicles depends on the amount of FA attached to the surface of the vehicle, with moderate FA coverage (50%) being more cytotoxic than high FA coverage. It was found that cytotoxicity is not affected by surface attached PEG, but if the drug-bound delivery vehicle is equipped with both FA and a thermoresponsive polymer, the resulting cytotoxicity is an order of magnitude greater than that of free doxorubicin. The investigation uncovered the effects of important surface attached groups on the cellular uptake and cytotoxicity of doxorubicin delivered by DNA-capped gold nanoparticles to cells growing in culture.

EXPERIMENTAL SECTION

Except where otherwise specified, all materials were purchased from Sigma-Aldrich, St. Louis, MO. All oligonucleotides were purchased from Integrated DNA Technologies, Coralville, IO. Single- and double-stranded DNA-functionalized gold nanoparticles, **1a**-AuNP and **1ab**-AuNP, were synthesized and characterized as previously reported.[30,31] Mass spectrometric analyses were provided by Novatia, Newtown, PA (oligonucleotides) and Cosmic, Norfolk, VA (FA and its derivatives).

Nuclear Magnetic Resonance (NMR). NMR spectroscopy was performed using Bruker DPX-300 and Bruker DRX-500 instruments, with dimethyl sulfoxide (DMSO)-d_6 as the solvent. Spectra were referenced internally to the DMSO-d_6 signals at 2.50 and 39.51 for ^{1}H and ^{13}C NMR, respectively. To prepare samples for analysis, 0.005 g (for ^{1}H NMR) or 0.039 g (for ^{13}C NMR) of FA or *N*-hydroxysuccinimide (NHS)-FA was dissolved in 0.6 mL DMSO-d_6 and added to a clean dry NMR tube, which was then capped and protected from light. NMR integral errors are ±10%.

Fourier Transform Infrared Spectroscopy (FT-IR). FT-IR spectra were collected from 650 to 4000 cm^{-1} using a Thermo Scientific Nicolet 6700 instrument equipped with a diamond smart iTR attenuated internal reflectance accessory, with a N_2 (l) cooled MCT-A detector. Samples were drop-cast as dried powders.

UV–vis Spectrophotometry. A Varian Cary 100 Bio UV–vis spectrophotometer was used to measure absorption spectra (with baseline correction) in the 200–900 nm region.

Synthesis of NHS-Activated Folic Acid (NHS-FA). Folic acid 261 mg (0.592 mmol) was stirred under an argon atmosphere in 10.0 mL anhydrous DMSO. After the FA was fully dissolved, 134 mg of *N,N′*-dicyclohexylcarbodiimide (DCC, 0.651 mmol) and 74.9 mg NHS (0.651 mmol) were added and the reaction mixture was allowed to proceed overnight at RT under argon in the dark. The dicyclohexylurea (DCU) precipitate which formed was removed using a 0.22 μm syringe filter and the filtrate was divided into equal (2.5 mL) volumes. Each volume of the filtrate was dropwise added to 12.5 mL of an ice cold acetone/anhydrous diethyl ether (30:70) mixture while stirring, and the solid that formed, referred to as "NHS-FA reaction product", was recovered and washed three times (centrifugation at $10^4 \times g$) with cold ether. The residual ether was removed under vacuum to give NHS-FA reaction product which ^{1}H NMR (vide infra) showed to contain 66% NHS-FA and 34% unreacted FA. The yellow product was stored at −20 °C until use. ^{1}H NMR (300 MHz, DMSO-d_6): δ 8.65 (1.0 H, s, CH), 8.13 (0.4 H, dd, NH), 7.64 (2.1 H, m, CH), 7.00 (1.4 H, m, NH), 6.65 (2.0 H, m, NH), 4.48 (2.2 H, d, CH_2), 4.35 (0.4 H, m, CH), 2.80 (2.6 H, s CH_2), 2.31 (0.6 H, m, CH_2). ^{13}C NMR (75 MHz, DMSO-d_6): δ 174.0, 173.8, 166.6, 153.8, 150.9, 148.6, 129.2, 128.0, 121.2, 111.2, 51.5, 45.9, 30.5, 170.2, 25.3. FT-IR (neat): 1813 cm^{-1} (ν C═O of NHS), 1785 cm^{-1} (ν C═O of NHS), 1694 cm^{-1} (ν C═O of −COOH), 1638 cm^{-1}(ν C═O of amide), 1605 cm^{-1} (δ $-NH_2$), 1489 (phenyl ring). ESI-MS: exact mass for NHS-FA, $C_{23}H_{22}N_8O_8$ Na^+: 561.1452; observed mass: 561.1451.

Synthesis of 1b-Folic Acid (1b-FA). The NHS-FA reaction product, 31.4 mg, containing 36.97 μmol NHS-FA, was fully dissolved in 300 μL DMSO and the resulting solution was dropwise added to a solution containing the 5′-amino DNA oligomer, **1b**-amine (0.74 μmol, ε_{260} = 201 500 M^{-1} cm^{-1}) in 3 mL of 100 mM bicarbonate buffer (pH 8.4). The reaction was allowed to proceed for 48 h with stirring in the dark, after which time **1b**-FA (plus unreacted **1b**-amine) was recovered by ethanol precipitation followed by drying under vacuum. The crude product was stored at −20 °C until its subsequent purification using IE-HPLC.

Purification of **1b**-FA was carried out at 55 °C using an Agilent 1200 series HPLC instrument equipped with an anion exchange analytical column (Dionex). A 10 min gradient from 0–60% B was employed at a flow rate of 1.2 mL/min (solvent A: 0.01 M tris HCl, 20% acetonitrile, pH 8.0, and solvent B: 0.01 M tris HCl, 20% acetonitrile, 0.33 M $NaClO_4$, pH 8.0). A typical purification involved ∼500 μL of total solution which was separated using an automated injector with ∼1–5 μL per

injection with detection by absorbance at 260 and 360 nm. Under these conditions, **1b**-amine and **1b**-FA eluted with baseline separation at 7.48 and 8.12 min, respectively. The product in the pooled **1b**-FA fractions was recovered by ethanol precipitation. Typically, 5.0 mL of a purified **1b**-FA solution, 500 μL 3 M sodium acetate (pH 5.2), and 12.5 mL ice cold ethanol were cooled on ice for 30 min, followed by centrifugation for 30 min at 10 000 × *g*. The precipitate containing **1b**-FA was washed at least three times with 70% ethanol, dried in a vacuum, and stored at −20 °C until needed. Electrospray ionization-mass spectrometry (ESI-MS): exact mass for **1b**-FA: 6441; observed mass: 6440.6.

Synthesis of 1ab-FA-AuNP, 1ab-PEG(9)-AuNP, and 1ab-PEG(18)-AuNP. These double stranded DNA-AuNP were synthesized and characterized as previously reported,[30,31] except that the complementary oligonucleotides used were **1b**-FA, **1b**-PEG(9), and **1b**-PEG(18) rather than **1b**. Both **1b**-PEG(9) and **1b**-PEG(18) were purchased from Integrated DNA Technologies, Coralville, IO, and used without modification.

Synthesis of pNIPAAm-*co*-pAAm Copolymer Capped AuNP (p-AuNP). A copolymer consisting of *N*-isopropylacrylamide (NIPAAm) and acrylamide (AAm) units were prepared via an atom transfer radical polymerization at a NIPAAm:AAm monomer ratio of 90:10 using a disulfide initiator.[32] This pNIPAAm-*co*-pAAm polymer (*p*) had a low critical solution temperature (LCST, T_C) of 51 °C, and a molecular weight of ∼290 000 (PDI = 1.12) in disulfide form.[32] Successful synthesis of a *p* with a T_C of 51 °C was achieved. The *p*-modification of AuNP was prepared as recently reported.[32] The disulfide *p* was incubated with excess 100 mM tris(2-carboxyethyl)phosphine hydrochloride (TCEP) for 30 min at room temperature which reduced the disulfide to the thiol form of the polymer (*p*). Next, *p* was added to citrate stabilized AuNP at 12.5:1 molar ratio (polymer/AuNP), and the resulting solution was incubated in the dark overnight at RT. The *p*-AuNP was recovered by centrifugation and washed three times using phosphate buffered saline (PBS) to remove any unreacted *p* present in solution.

Synthesis of 1ab/p-AuNP. Using the recently reported salt aging procedure,[32] AuNP were combined with a 300 molar excess of the thiolated DNA 35-mer (**1a**). After 12 h, the phosphate buffer concentration was adjusted to 10 mM. At intervals of 6 h, the NaCl concentration was gradually increased to a final concentration of 300 mM after ∼3 days. At the 25 mM NaCl salt aging step, the thiol form of the polymer was added at 12.5:1 molar ratio (polymer/AuNP), and the salt aging process continued. After completing salt aging, the **1a**/*p*-AuNP was isolated by centrifugation, washed, and then hybridized with **1b** as previously reported,[30,31] to produce **1ab**/*p*-AuNP. For all DNA-capped AuNP, determination of the number of **1ab** bound per AuNP was performed using fluorescence spectroscopy as previously described.[30,31] The number of DNA duplexes bound per AuNP was measured to be 64.5 ± 2.5 for **1ab**-AuNP and 53.9 ± 10.6 for **1ab**/*p*-AuNP, revealing that incubation with *p*-capped AuNPs during salt aging does not significantly impact the loading of **1a** at the AuNP surface.

DOX Loading for 1ab-AuNP, 1ab-FA-AuNP, 1ab-PEG(9)-AuNP, 1ab-PEG(18)-AuNP, and 1ab/p-AuNP. To achieve drug loading, each AuNP (except **1ab**/*p*-AuNP) was incubated for 40 min at RT with DOX at a loading ratio of 1 DOX molecule per DNA binding site. For **1ab**/*p*-AuNP, DOX loading was performed at 53 °C to promote complete drug loading in the presence of the polymer. Prior to incubation with AuNP, DOX concentrations were determined optically using ε_{480} = 11 500 M^{-1} cm^{-1}.

Dynamic Light Scattering (DLS). All measurements of hydrodynamic diameter (D_h) were obtained using A Malvern Zetasizer Nano ZS system, equipped with a 633 nm laser source and a backscattering detector at 173°. Prior to measurement, samples were filtered using a 0.22 μm filter. Each reported D_h value is an average of multiple measurements (>3), each of which consisted of >11 data collection runs. CONTIN data analysis was utilized, and size averaged distributions are reported.

Confocal Microscopy. Confocal images were acquired using a Zeiss LSM 710 confocal microscope equipped with multiple laser lines. Zen software was used for data analysis. To prepare samples, 1.25 × 10^4 cells were seeded in pre-equilibrated Mat-tek glass bottom culture dishes in 250 μL of RPMI+ (RPMI media deficient in folic acid, containing 10% fetal bovine serum (FBS), 100 μg/mL streptomycin, and 100 IU/mL penicillin), and were permitted to grow for 24 h. Media was then replaced with media containing 5 μM free DOX or delivery vehicle having 5 μM of loaded DOX. After a 24 h exposure time, the cells were washed three times with sterile PBS and permitted to recover for 1 h. Confocal images were then acquired using a brightfield channel and a DOX fluorescence channel (DOX λ_{ex} = 490 nm, λ_{em} = 565−615 nm). The displayed images include brightfield and merged (brightfield and DOX fluorescence) channels, with a 40 μM scale bar.

Cytotoxicity. In order to access the effects of the targeting vector, FA, cytotoxicity measurements were performed using a modification of the previously reported[31] procedures. Briefly, neuroblastoma (SK-N-SH) cells were maintained in MEM+ (MEM media containing 10% fetal bovine serum, FBS, 100 μg/mL streptomycin, and 100 IU/mL penicillin) in an incubator humidified at 37 °C and 5% CO_2 atmosphere. In order to deplete the cells of folic acid and thus promote FA targeting, beginning one passage before the cytotoxicity experiments, normal media was replaced with RPMI+ (RPMI media that is deficient in folic acid, containing 10% FBS, 100 μg/mL streptomycin, and 100 IU/mL penicillin). Stock solutions of drug or drug loaded particle were prepared at 0.005, 0.05, 0.5, and 5 μM DOX, with a DOX/binding site ratio of 1:1. Cells were plated with 6 replicate wells per condition, in 96-well microplates at 5 × 10^4 cells/mL, and were permitted to grow for 24 h. RPMI+ was then replaced with RPMI+ containing drug at the indicated concentrations. In this study multiple exposure (E) and recovery times were used (R), Table 1. Viability was then evaluated using a CCK-8 assay (Dojindo Molecular Technologies, Inc., Rockville, MD). Percent inhibition (%*I*) was calculated as reported previously and the error on %*I* was calculated as a standard deviation of replicate measurements.

■ ASSOCIATED CONTENT

Supporting Information

Additional data including $^1H/^{13}C$ NMR assignments, FTIR spectra, ESI-MS/UV−visible spectra, and hydrodynamic diameters. This material is available free of charge via the Internet at http://pubs.acs.org.

AUTHOR INFORMATION

Corresponding Authors

*E-mail: mmmaye@syr.edu. Phone: 315-443-2146. Fax: 315-443-4070.

*E-mail: jcdabrow@syr.edu. Phone: 315-443-4601. Fax: 315-443-4070.

Notes

The authors declare no competing financial interest.

ACKNOWLEDGMENTS

The authors would like to thank Deborah Kerwood, Yi Shi, Jerry Goodisman, and Yan Yeung Luk (Department of Chemistry, Syracuse University) for their helpful discussions concerning this work.

REFERENCES

(1) Murphy, C. J., Gole, A. M., Stone, J. W., Sisco, P. N., Alkilany, A. M., Goldsmith, E. C., and Baxter, S. C. (2008) Gold nanoparticles in biology: beyond toxicity to cellular imaging. *Acc. Chem. Res. 41*, 1721−1730.

(2) Fadeel, B., and Garcia-Bennett, A. E. (2010) Better safe than sorry: understanding the toxicological properties of inorganic nanoparticles manufactured for biomedical applications. *Adv. Drug Delivery Rev. 62*, 362−374.

(3) Dreaden, E. C., Mackey, M. A., Huang, X., Kangy, B., and El-Sayed, M. A. (2011) Beating cancer in multiple ways using nanogold. *Chem. Soc. Rev. 40*, 3391−3404.

(4) Rana, S., Bajaj, A., Mout, R., and Rotello, V. M. (2012) Monolayer coated gold nanoparticles for delivery applications. *Adv. Drug. Delivery Rev. 64*, 200−16.

(5) Giljohnn, D. A., Seferos, D. S., Danial, W. L., Massich, M. D., Patel, P. C., and Mirkin, C. A. (2010) Gold nanoparticles for biology and medicine. *Angew. Chem., Int. Ed. Engl. 49*, 3280−94.

(6) Mieszawaka, A. J., Mulder, W. J., Fayad, Z. A., and Cormode, D. P. (2013) Multifunctional gold nanoparticles for diagnosis and therapy of disease. *Mol. Pharmacol. 10*, 831−47.

(7) Liu, A., and Ye, B. (2013) Application of gold nanoparticles in biomedical researches and diagnosis. *Clin. Lab. 59*, 23−36.

(8) Liu, J., Yu, M., Zhou, C., Yang, S., Ning, X., and Zheng, J. (2013) Passive tumor targeting of renal-clearable luminescent gold nanoparticles: long tumor retention and fast normal tissue clearance. *J. Am. Chem. Soc. 135*, 4978−4981.

(9) Feng, S. S., and Chien, S. (2003) Chemotherapeutic engineering: Application and further development of chemical engineering principles for chemotherapy of cancer and other diseases. *Chem. Eng. Sci. 58*, 4087−4114.

(10) Yeh, E. T. H., and Bickford, C. L. (2009) Cardiovascular complications of cancer therapy. *J. Am. Coll. Cardiol. 53*, 2231−2247.

(11) Cai, W. (2008) Applications of gold nanoparticles in cancer nanotechnology. *Nanotechnol. Sci. Appl. 1*, 17−32.

(12) Kim, C. k., Ghosh, P., and Rotello, V. M. (2009) Multimodal drug delivery using gold nanoparticles. *Nanoscale 1*, 61−7.

(13) Kumar, A., Zhang, X., and Liang, X. J. (2013) Gold nanoparticles: emerging paradigm for targeted drug delivery. *Biotechnol. Adv. 31*, 593−606.

(14) Powell, A. C., Paciotti, G. F., and Libutti, S. K. (2010) Colloidal gold: a novel nanoparticle for targeted cancer therapeutics. *Methods Mol. Biol. 624*, 375−84.

(15) Kumar, A., Ma, H., Zhang, X., Huang, K., Jin, S., Liu, J., Wei, T., Cao, W., Zou, G., and Liang, X.-J. (2012) Gold nanoparticles functionalized with therapeutic and targeted peptides for cancer treatment. *Biomaterials 33*, 1180−1189.

(16) Arosio, D., Manzoni, L., Araldi, E. M., and Scolastico, C. (2011) Cyclic RGD functionalized gold nanoparticles for tumor targeting. *Bioconjugate Chem. 22*, 664−72.

(17) Nasrolahi Shirazi, A., Mandal, D., Tiwari, R. K., Guo, L., Lu, W., and Parang, K. (2013) Cyclic peptide-capped gold nanoparticles as drug delivery systems. *Mol. Pharmacol. 10*, 500−11.

(18) Cheng, Y., Doane, T. L., Chuang, C. H., Ziady, A., and Burda, C. (2014) Near infrared light-triggered drug generation and release from gold nanoparticle carriers for photodynamic therapy. *Small*, DOI: 10.1002/smll.201303329.

(19) Cheng, Y., Meyers, J. D., Broome, A. M., Kenney, M. E., Basilion, J. P., and Burda, C. (2011) Deep penetration of a PDT drug into tumors by noncovalent drug-gold nanoparticle conjugates. *J. Am. Chem. Soc. 133*, 2583−91.

(20) Meyers, J. D., Doane, T., Burda, C., and Basilion, J. P. (2013) Nanoparticles for imaging and treating brain cancer. *Nanomedicine (London) 8*, 123−43.

(21) Cheng, Y., Meyers, J. D., Agnes, R. S., Doane, T. L., Kenney, M. E., Broome, A.-M., Burda, C., and Basilion, J. P. (2011) Addressing brain tumors with targeted gold nanoparticles: a new gold standard for hydrophobic drug delivery? *Small 7*, 2301−2306.

(22) Leamon, C. P., and Low, P. S. (2001) Folate-mediated targeting: from diagnostics to drug and gene delivery. *Drug Discovery Today 6*, 44−51.

(23) Zhao, X., Li, H., and Lee, R. J. (2008) Targeted drug delivery via folate receptors. *Expert Opin. Drug Delivery 5*, 309−19.

(24) Llevot, A., and Astruc, D. (2012) Applications of vectorized gold nanoparticles to the diagnosis and therapy of cancer. *Chem. Soc. Rev. 41*, 242−57.

(25) Drbohlavova, J., Chomoucka, J., Adam, V., Ryvolova, M., Eckschlager, T., Hubalek, J., and Kizek, R. (2013) Nanocarriers for anticancer drugs—new trends in nanomedicine. *Curr. Drug Metab. 14*, 547−64.

(26) Low, P. S., Henne, W. A., and Doorneweerd, D. D. (2008) Discovery and development of folic-acid-based receptor targeting for imaging and therapy of cancer and inflammatory diseases. *Acc. Chem. Res. 41*, 120−129.

(27) Leamon, C. P., and Low, P. S. (1991) Delivery of macromolecules into living cells: A method that exploits folate receptor endocytosis. *Proc. Natl. Acad. Sci. U.S.A. 88*, 5572−5576.

(28) Gautier, J., Allard-Vannier, E., Munnier, E., Soucé, M., and Chourpa, I. (2013) Recent advances in theranostic nanocarriers of doxorubicin based on iron oxide and gold nanoparticles. *J. Controlled Release 169*, 48−61.

(29) Cheng, J., Gu, Y. J., Cheng, S. H., and Wong, W. T. (2013) Surface functionalized gold nanoparticles for drug delivery. *J. Biomed. Nanotechnol. 9*, 1362−9.

(30) Alexander, C. M., Dabrowiak, J. C., and Maye, M. M. (2011) DNA-capped nanoparticles designed for doxorubicin drug delivery. *Chem. Commun. 47*, 3418−3420.

(31) Alexander, C. M., Dabrowiak, J. C., and Maye, M. M. (2012) Investigation of the drug binding properties and cytotoxicity of DNA-capped nanoparticles designed as delivery vehicles for the anticancer agents doxorubicin and actinomycin D. *Bioconjugate Chem. 23*, 2061−2070.

(32) Hamner, K. L., Alexander, C. M., Coopersmith, K., Reishofer, D., Provenza, C., and Maye, M. M. (2013) Using temperature sensitive smart polymers to regulate DNA-mediated nano assembly and encoded nano carrier drug release. *ACS Nano 7*, 7011−7020.

(33) Albanese, A., Tang, P. S., and Chan, W. C. W. (2012) The effect of nanoparticle size, shape, and surface chemistry on biological systems. *Annu. Rev. Biomed. Eng. 14*, 1−16.

(34) Blum, R. H., and Carter, S. K. (1974) Adriamycin. A new anticancer drug with significant clinical activity. *Ann. Int. Med. 80*, 249−59.

(35) Donaldson, M. H. (1972) Proceedings: Treatment of neuroblastoma—1972. *Proc. Natl. Cancer Conf. 7*, 605−9.

(36) Cheung, N. V., and Heller, G. (1991) Chemotherapy dose intensity correlates strongly with response, median survival, and median progression-free survival in metastatic neuroblastoma. *J. Clin. Oncol. 9*, 1050−8.

(37) Dixit, V., Van den Bossche, J., Sherman, D. M., Thompson, D. H., and Andres, R. P. (2006) Synthesis and grafting of thioctic acid-PEG-folate conjugates onto Au nanoparticles for selective targeting of folate receptor-positive tumor cells. *Bioconjugate Chem. 17*, 603−609.
(38) Aronov, O., Horowitz, A. T., Gabizon, A., and Gibson, D. (2003) Folate-targeted PEG as a potential carrier for carboplatin analogs. Synthesis and in vitro studies. *Bioconjugate Chem. 14*, 563−574.
(39) Zhang, K., Wang, Q., Xie, Y., More, G., Sega, E., Low, P. S., and Huang, Y. (2008) Receptor-mediated delivery of siRNAs by tethered nucleic acid base-paired interactions. *RNA 14*, 577−583.
(40) Tewey, K. M., Rowe, T. C., Yang, L., Halligan, B. D., and Liu, L. F. (1984) Adriamycin-induced DNA damage mediated by mammalian DNA topoisomerase II. *Science 226*, 466−468.
(41) Eustis, S., and El-Sayed, M. A. (2006) Why gold nanoparticles are more precious than pretty gold: Noble metal surface plasmon resonance and its enhancement of the radiative and nonradiative properties of nanocrystals of different shapes. *Chem. Soc. Rev. 35*, 209−217.